Effect of Unipolar Arcing on W Erosion During the Metal Tile Campaign in DIII-D

I. Bykov[a,*], C.P. Chrobak[b], T. Abrams[b], D.L. Rudakov[a], E.A. Unterberg[c], W.R. Wampler[d], E.M. Hollmann[a], R.A. Moyer[a], J.A. Boedo[a], B. Stahl[b], E.T. Hinson[e], J.H. Yu[a], C.J. Lasnier[f], M. Makowski[f], A.G. McLean[f]

[a] *University of California (San Diego), La Jolla, USA*
[b] *General Atomics, P.O. Box 85608, San Diego, CA, 92186-5608, USA*
[c] *Oak Ridge National Laboratory, Oak Ridge, TN, 37830, USA*
[d] *Sandia National Laboratories, Albuquerque, NM, and Livermore, CA, USA*
[e] *University of Wisconsin-Madison, Wisconsin, WI, 53706, USA*
[f] *Lawrence Livermore National Laboratory, Livermore, CA 94550, USA*

Unipolar arcing may be a locally dominant surface erosion mechanism in tokamaks with metallic PFCs. Recently, Metal Tile Campaign has been conducted at DIII-D: two toroidally continuous tile arrays with 5 cm wide W-coated TZM inserts were installed in graphite tiles in the lower divertor, one on the floor and one on the shelf. They were exposed for the total of ~500 discharges, an equivalent of plasma time on W surfaces (with I_p >0.5 MA) ~10^3 s. Arcing was monitored in situ with WI (400.9 nm) filtered camera and filterscopes and showed that: (i) arcing only occurred during ELMs and disruptions, (ii) arcing rate was much lower on the floor than on the shelf insert, and (iii) arcing had a cut-off intra-ELM heat flux density about 2 MW/m^2. About half of arc tracks had large 10° pitch angle and probably were produced during disruptions. Such tracks were only found on the shelf. Moderate toroidal variation of the arc track density and W erosion with nearly n=1 pattern has been measured. The total amount of W removed by arcing from ~4% of the affected W area was estimated ~0.8×10^{21} at., about half of the total amount of W eroded and redeposited outside the inserts $(1.8\pm0.9)\times10^{21}$ at.

Keywords: DIII-D, arcing, tungsten, erosion

INTRODUCTION

Unipolar arcing is an important local surface erosion mechanism in controlled fusion devices. Arcing is routinely observed in machines with graphite first wall but owing to the high sputtering and chemical erosion of C it usually is not the dominant mechanism. In machines with metal first wall aiming at reduced plasma contamination and wall erosion by atomic sputtering arcing can be a much stronger local erosion source. It was demonstrated more than 40 years ago that under edge plasma conditions unipolar arcing can lead to several orders of magnitude higher erosion rates than simple atomic sputtering [1]. This makes the arcs of primary concern for future fusion devices with high-Z wall like ITER when the wall impurity source has to be minimized.

In present experiments arcing can complicate interpretation of in situ and campaign integrated erosion measurements and has to be avoided. Arcing has been studied in many machines either in dedicated experiments with small-scale test samples exposed in a limited number of discharges with controlled parameters [2–4] or performing shutdown in-vessel surveys of permanently installed components assessing integrated effect of arcing after the whole campaign [5, 6]. Still, there is no arc avoidance strategy proposed compatible with high-performance tokamak operation.

In June-July 2016, a short-term Metal Tile Campaign (MTC) has been conducted at DIII-D to study W sourcing in the divertor, its migration, transport, and core contamination, and to explore high-Z wall compatibility with high performance plasmas. In this work we report on observations of arcing on metal surfaces and their effect on material erosion in the divertor of DIII-D during operations with partially W-covered divertor plasma facing components (PFCs).

*Corresponding author: ibykov@ucsd.edu

Table I: Diagnostics relevant for arc detection and imaging

Diagnostic	FPS	Filter	Resolution/Area imaged	Active period, shots
DiMES-TV	100	WI 400.9 nm	0.8 mm/px, 5° tor.	260
Fast camera	5k	610 nm	4 mm/px, 30° tor.	200
Filterscope	50k	WI 400.9 nm	3 cm^2, 2 spots on each ring	480, whole campaign

EXPERIMENTAL

DIII-D is a divertor tokamak with minor radius a=0.67 m and major R=1.67 m [7], with PFCs made of ATJ graphite conditioned by boronizations. For MTC, two toroidally continuous 5 cm wide W-coated TZM (Mo alloy with 0.50% Titanium and 0.08% Zirconium) tile inserts (rings) have been installed on the floor near the pump entrance and on the shelf. The floor insert was coated by chemical vapor deposition (CVD) of WF_6 gas, measurements on a test sample showed ~12 μm layer thickness, and the shelf insert was coated by electron-beam induced physical vapor deposition (PVD), the layer thickness was 1-2 μm.

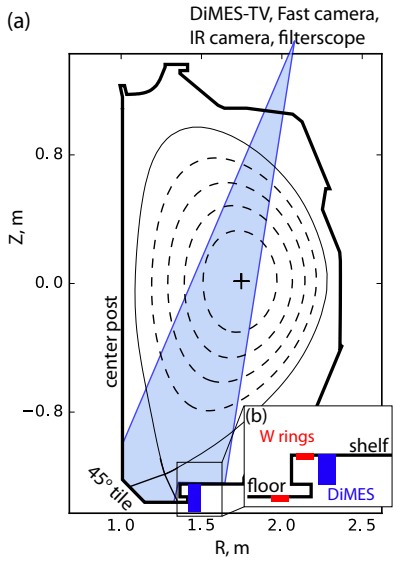

Figure 1: Schematic view of the DIII-D poloidal cross section with locations of divertor diagnostics (a) and inset showing locations of the shelf and floor W rings and DiMES (b). The cameras can see the shelf ring and only about half of the poloidal extent of the floor ring due to shadowing by the shelf.

Fig. 1 schematically shows outline of the DIII-D first wall, locations of divertor diagnostics, W rings and Divertor Materials Evaluation Station (DiMES) Ref. [8]. For more details see Fig 1 in Ref. [9]. Measurement of infra red (IR) radiation in the range 3-5 μm for calculation of incident heat flux profile $q_\perp$ across a full-C section of the divertor was done with an IR camera. It was operated in fast line scan mode with framing rate up to 12 kHz thus able to capture intra-ELM heat flux evolution. An array of filtered photomultipliers (filterscopes) with several poloidal chords measures main ion and impurity emission across the divertor at sampling rate 50 kHz. The Divertor Materials Evaluation System (DiMES) [8] allows up to ∅5 cm sample exposure flush with the lower divertor surface and sample exchange on inter-shot time scale. During MTC, graphite samples were exposed at DiMES for studies of local W migration with outer strike point (OSP) kept on the outer W row [9].

Two visible-range filtered cameras were monitoring the metal inserts: a slow WI-filtered (DiMES-TV) and a fast camera, imaging emission from D_2 Fulcher band probably with some contribution from C_2 Swan band. The latter technique has proven efficient for imaging small UFOs like particles or droplets. With spatial resolution ~4 mm/px this system could be useful for imaging emission from arc ejecta and part of broadband emission from arcs. The frame rate was lower than 27 kFPS previously applied for arc imaging [10], this allowed to store data for entire discharge >6 s and potentially record single-frame arc footprints being unable to resolve the arc-track evolution. Four additional filterscope chords have been installed to monitor each of the W rings (two chords per ring at different but close toroidal locations) and provide background subtracted photon fluxes of neutral W line at 400.9 nm using a recently introduced technique [11]. Summary of diagnostics relevant for in situ arc detection is given in Table I.

RESULTS AND DISCUSSION

In situ arc detection

The Metal Tile Campaign at DIII-D was conducted in June-July 2016 [12]. It spanned total of ∼480 discharges (I_p>0.5 MA) with integrated exposure of the W surfaces to diverted plasma 350 s on the shelf and 660 s on the floor. Most of the discharges were in H-mode with attached OSP placed on either of the two rings. About 20% of developed H-mode discharges were terminated by a disruption.

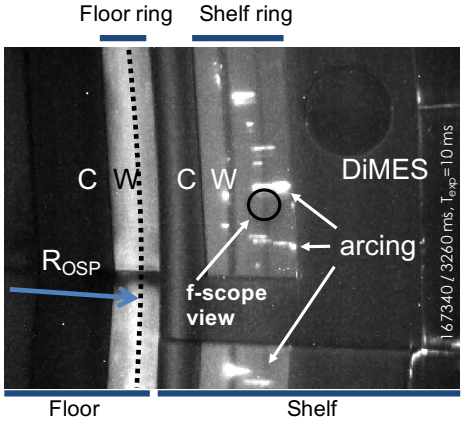

Figure 2: Example of arcing on W during an ELM crash. OSP is on the floor ring but arcing is only seen on the shelf. Some wall elements and WI filterscope collection area are shown. In diverted discharges the arcs propagate in the $\vec{B} \times \vec{J}_{arc}$ direction nearly radially because the radial B-field component is small, leading to pitch angle ∼3°.

Multiple observations of arcing events were made in situ on the shelf ring with DiMES-TV, arcing rate on the floor ring was much lower than on the shelf. WI filterscopes were sensitive to all fast transients like ELMs, disruptions and arcing. Arcing was expected during these transients [10] therefore the arc signals had to be discriminated from other events. This was done using differential signal from two shelf WI filterscopes near DiMES. One of the filterscopes' spots was within the camera field of view, cf. Fig. 2,4 and the camera was used to calibrate this technique. It was confirmed that the arcing only occurred during ELMs or during disruptions. This method could not be used for counting arcs since the arcs were synced with ELMs and there could be more than one at the same time in the filterscope's view. This has been done using the camera.

An example of a camera frame capturing arcing is shown in Fig. 2. The tracks are aligned radially owing to the small radial B-field component. With OSP on the floor ring no arcs can be seen there but multiple arcs are on the shelf. This was typical for the whole campaign and probably had two reasons.

- The W coating was thinner on the shelf which under similar conditions makes it more prone to arcing. Multi machine experience of operations with W PFCs shows that under similar plasma conditions arcing may favor thinner W coatings. In AUG with full W divertor arcing was reported on the inner marker Tile 5 (inboard from ISP) with W coverage ∼300 nm [13] to be compared with 500-600 nm marker layers in the outer divertor and 1.5 μm under OSP. Previously reported DIII-D studies of metals' erosion on DiMES consistently revealed arcing on ∼100 nm thick deposited W layers on graphite [4].

- Splitting of the heat flux footprint during ELMs was leading to higher power deposition further away from the OSP on the shelf insert. In the shown example the arcing occurred on the shelf ring in the SOL at ψ_n ≈1.04 during a large ELM with peak heat flux on the floor and shelf rings respectively 6 and 9 MW/m^2. The resulting stored energy drop was 240 kJ in contrast to ∼40 kJ and 4 MW/m^2 at OSP during regular ELMs in the same discharge.

Over the whole campaign, excluding disruptions, large infrequent ELMs with high $q_\perp$ either at the end of ELM-free phases or RMP ELM-suppressed periods were causing most intense arcing . The highest arcing rate per ELM on the floor ring was 0.2 cm^{-2} with $q_\perp$ ≈5 MW/m^2.

Arcing rates on W surfaces were counted using DiMES-TV images and plotted as function of ELM power $q_\perp$, Fig. 3 . The zero count rates are averaged over many ELMs where no arcing was detected. The non-zero rates are

from individual ELMs with arcs. Arcing on the shelf W coating had lower ELM power threshold ~1.8 MW/m^2 vs. ~2.4 MW/m^2 on the floor owing probably to its lower thickness and/or different coating method. Additional data has been added from a separate DiMES experiment where a ∅5 cm sample with similar surface to that of the shelf W ring was exposed in a limited number of discharges. The DiMES data lines up with that from the shelf insert showing that the result is reproducible and longer term coating performance can be estimated based in a single experiment test. Disruptions could adversely affect W surface conditions probably adding C and O. In a series of discharges that terminated by disruptions in the following discharge the arcing rate per ELM f_{arc}^{ELM} increased on the floor ring to 0.4 cm^{-2} at $q_\perp$=3.6 MW/m^2 and on the shelf to 0.3 cm^{-2} at $q_\perp$=2.6 MW/m^2.

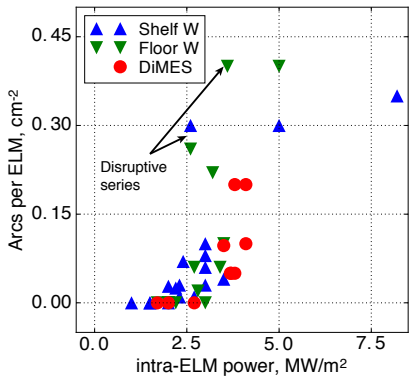

Figure 3: Areal density of arcs per ELM vs. peak intra-ELM heat flux on the W rings during MTC and on DiMES in a dedicated experiment. Arcing rate increased in discharges following disruptions.

The fast camera with a D filter could not spatially resolve the arcs during ELMs. From the slow camera images, there were no detectable macroscopic ejecta (dust or droplets) produced by arcs thus there was nothing that could indicate arcing for the lower resolution camera. Nevertheless, during disruptions there were multiple micro particles ejected from C surfaces including far outer shelf, bottom of the center post and the 45° tile where arcs are usually found during shutdown entries. During the shutdown, multiple arc damage was found in that area reassuring that C particle ejection seen during disruptions was likely due to arcing.

In all scenarios there was no inter-ELM or L-mode arcing detectable. During disruptions, the W-filtered camera saturated but the WI filterscopes showed intense arcing. Evidence of disruption-induces arcing was found during post mortem analysis

Post mortem tile analysis

Full set of tiles with the metal insets and some of the graphite divertor tiles including those from the 45° tile were removed from the vessel after the experiment for post mortem analysis. This included electron microscopy (SEM) with X-ray microanalysis, surface profilometry, and ion beam analysis (IBA) of W and C on DiMES C samples [14].

On the shelf insert multiple arc tracks were visible by unaided eye. The floor insert had over factor 10 fewer arc tracks which was also confirmed by visible and electron microscopy. Fig. 4a shows a post mortem image of the shelf insert near DiMES with multiple arc tracks. The dark line on the W insert is due to C deposition in recessed surface areas due to operation with rev. B_t. Arc damage was predominantly found on the shelf inserts, therefore analysis focused on the tracks found on the shelf rings. Arc tracks on bare W microscopically consist of individual holes (Type I, see Ref. [15]) and in areas partly covered by redeposited C they are continuous (Type II) and up to 1 cm long.

In presence of strong magnetic field the arcs are known to move in the *retrograde* direction $\vec{B} \times \vec{J}$ i.e. opposite to the direction of Lorenz force on net arc current. This property makes it possible to reconstruct the local B-field direction at the time when arc tracks appeared. Two kinds of arc tracks can be seen in Fig. 4b: nearly radial with pitch angle of a few degrees, and with pitch angle about 10°. The low-pitch tracks must have appeared during controlled phases of diverted discharges when the field line pitch angle is small. Tracks with the angle ~10° must have appeared during disruptions, similar to experiment Ref. [2]. The two preferential inclinations are due to forward and reversed B_t.

Equilibrium evolution during a typical disruption which were Vertical Displacement Events (VDEs) calculated with fast EFIT is shown in Fig. 5(a). The field-line pitch angle in the middle of the shelf ring changes from 3° to 7° as the VDE develops. This is similar to what was observed on DiMES samples of W fuzz during dedicated VDE

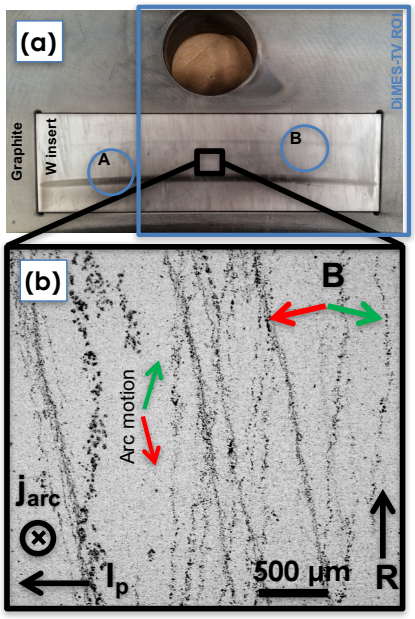

Figure 4: (a) Post mortem overview of the shelf insert near DiMES. Two WI filterscope spots' projections are shown with circles A and B. Part of the image inside the blue frame is also seen by DiMES-TV camera. Multiple arc tracks with different pitch angle are visible. (b) SEM close up with indication of Ip, normal and reversed B_t, and arc current. The respective arc motion directions are indicated for tracks with high pitch angle ~10°.

experiment Ref. [2]. The shelf nose acts as a toroidal limiter shadowing the floor hence no damage on the floor ring. Time evolution of I_p and stored energy during this disruption are shown in Fig. 5(b). Typically, these were Type II "cold" VDEs characterized by high poloidal halo current [16, 17] and radiative thermal quench (TQ) preceding current quench (CQ) [18] in contrast to "hot" VDEs in Ref. [2]. Cold VDEs had heat flux on the shelf $q_\perp \approx 2$ MW/m^2, similar to a typical ELM but lasting up to a few ms. There are two peaks in the WI signal crossing the "arcing" threshold in the beginning of TC and CQ, typical for most of MTC disruptions indicating that even cold VDEs promoted intense arcing.

An important quantity is the total amount of W removed by arcing. Fig. 6a shows SEM image of a Type II arc track on the shelf insert. Circles A and B indicate regions within the track and nearby on undamaged surface from where X-ray spectra in (b) have been collected using 20 keV e-beam. W X-ray yield does not disappear at the bed of the track (Region B) which indicates that the arc did not burn through the whole W layer or at least some W was not removed. To find thickness of the remaining W layer the relative intensity of the most prominent in this range lines W $M_{\alpha 1}$ and Mo $L_{\alpha 1}$ has been simulated with PENELOPE Monte Carlo code for coupled electron-photon transport [19]. A simple geometry with thick elemental Mo substrate and top W layer (a proxy of shown in inset (a1) of Fig. 6) of varied thickness was used for simulation. Fig. 6c shows the results of this simulation for W layer thickness up to 3 μm. The calculated relative X-ray yield is best matched with the measured at model W layer thickness 0.7 μm. Thus, on average 0.8 μm of W has been removed. This is in accordance with the surface profilometry measurements of arc track profiles.

Fractional area of the surface damaged by arcing was estimated ~4%. Extrapolating to the total area of the shelf ring this amounts to 160 cm^2 and total removed 0.8×10^{21} at. W. This is about half of the total W redeposited poloidally outside W rings (and thus net eroded) measured by XRF - 550 mg or $(1.8\pm0.7)\times10^{21}$ at. W.

Probably, the W eroded by arcing did not contribute to the core contamination. After a single experiment which consisted of 23 (85 s of exposure with no evidence of arcing) similar non disruptive L-mode discharges with OSP on the shelf ring, W in a net deposition zone in the outer SOL ~5 cm outside shelf W ring has been measured with IBA on a DiMES sample [9, 14]. That W must have been flushed from the core and transported from outer midplane, its presence could not be explained by local erosion/transport simulations with ERO [9, 20]. For our consideration it is important that W accumulation in this region can serve to monitor net W erosion in configurations with OSP on the shelf ring. The areal density of W deposited on C at the same radial location has been measured with XRF after the whole campaign. There is a simple linear scaling of W deposition with OSP time on the shelf ring, Fig. 7, with average W deposition rate 4.9×10^{13} at./cm^2/s. This means that ELM- or disruption-induced W erosion did not add to the W deposited in that "monitoring" zone. This is possible if W eroded by arcs was promptly redeposited at

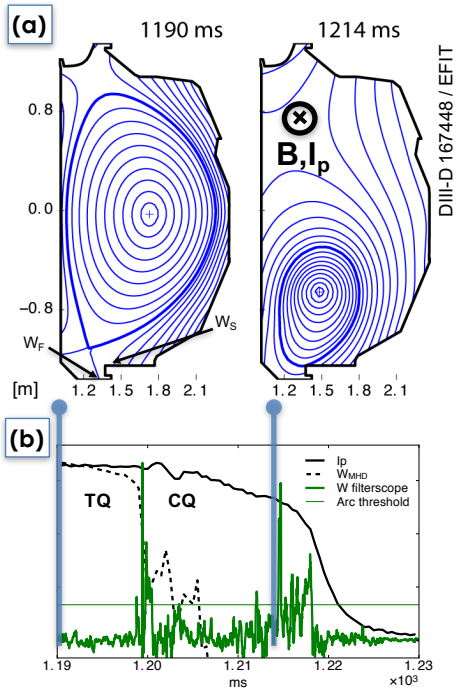

Figure 5: (a) EFIT reconstruction of downward plasma motion during a VDE disruption. The shelf with the W_s insert receive high heat flux but shadow the floor ring W_f. (b) Disruption evolution of plasma current I_p, stored energy W_{MHD}, and differential WI filterscope signal on the shelf. The latter has multiple peaks between thermal (TQ) and current quench (CQ) - a signature of intense arcing.

nearby PFCs.

The analysis presented so far focused on data from a single toroidal location near DiMES at 150°. It is important to verify to what extent this analysis is representative of the whole divertor. Fig. 8a shows toroidal distribution of the arc count rate on all the shelf inserts binned in 5 groups. Whole variation is about 50% of the maximum. The DiMES insert was located near the region most affected by arcing. The toroidal distribution of net W erosion (measured by XRF) in Fig. 8b shows a similar pattern. The n=1 structure of the distribution may suggest that there was an n=1 error field effect on the radial profiles at different toroidal locations affecting both the arc rate and the net erosion. This hypothesis can not be further substantiated. Presence of C spacers and diagnostic ports breaking toroidal continuity of the W surface (Fig. 8) could increase W surface contamination by redeposition in the typical downstream direction (toward higher toroidal angles) and promote arcing.

CONCLUSIONS

During the Metal Tile Campaign, arcing on W surfaces has shown to be a significant erosion mechanism but probably did not contribute to core contamination. Arcing occurred during ELMs and disruptions with more than 50% of events during disruptions. Arcing rate on W surfaces increased with ELM power and had threshold higher on the floor ring than on the shelf. The thicker floor ring was protected from disruption heat fluxes by the shelf. Resulting arc damage to the floor ring was negligible in comparison with the shelf. Arcing rate on the shelf was the same as on a test DiMES sample with similar W coating. This adds to credibility of small scale performance tests of high-Z coatings for future applications. ELM power scans can be used to select coatings with the arcing threshold compatible with plasma scenarios.

Acknowledgements. This work was supported in part by the U.S. Department of Energy under DE-FG02-07ER54917[a], DE-FC02-04ER54698[b], DE-AC05-00OR22725[c], DE-AC04-94-AL85000[d], DE-SC00013911[e], DE-AC05-

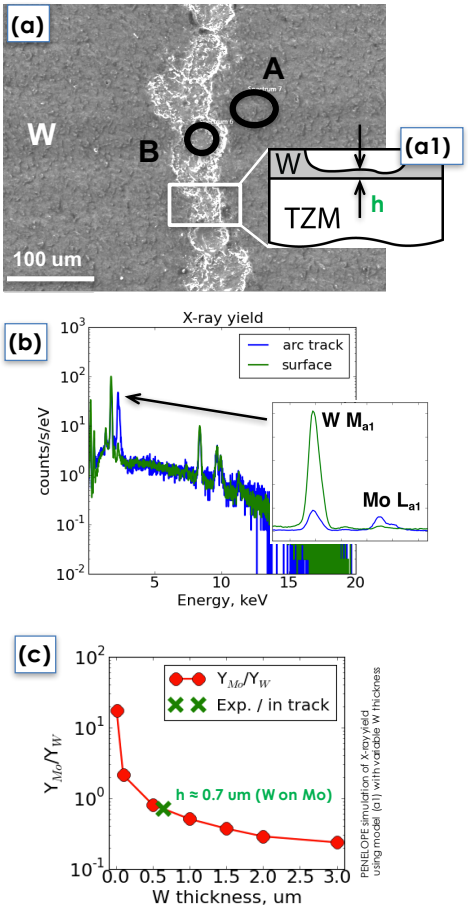

Figure 6: (a) Example of an arc track on the shelf W insert. X-ray spectra in (b) have been collected from regions **A** and **B** and relative Mo and W yield from **B** was matched by PENELOPE [19] simulation in (c) at assumed W layer thickness 0.7 μm.

07NA27344[f].

---

[1] G. H. Miley. Surface effects related to voltage breakdown in CTR devices. *Journal of Nuclear Materials*, 63:331 – 336, 1976.

[2] D. L. Rudakov, C. P. C. Wong, R. P. Doerner, et al. Exposures of tungsten nanostructures to divertor plasmas in DIII-D. *Physica Scripta*, 2016(T167):014055, 2016.

[3] M. Tokitani, S. Kajita, S. Masuzaki, et al. Exfoliation of the tungsten fibreform nanostructure by unipolar arcing in the LHD divertor plasma. *Nuclear Fusion*, 51(10):102001, 2011.

[4] D.G. Whyte, J.N. Brooks, C.P.C. Wong, et al. DiMES divertor erosion experiments on DIII-D. *Journal of Nuclear Materials*, 241:660 – 665, 1997.

[5] D.L. Rudakov, C.P. Chrobak, R.P. Doerner, et al. Arcing and its role in PFC erosion and dust production in DIII-D. *Journal of Nuclear Materials*, 438, Supplement:S805 – S808, 2013. Proceedings of the 20th International Conference on Plasma-Surface Interactions in Controlled Fusion Devices.

[6] A. Herrmann, M. Balden, M. Laux, et al. Arcing in ASDEX Upgrade with a tungsten first wall. *Journal of Nuclear Materials*, 390391:747 – 750, 2009. Proceedings of the 18th International Conference on Plasma-Surface Interactions in Controlled Fusion DeviceProceedings of the 18th International Conference on Plasma-Surface Interactions in Controlled Fusion Device.

[7] J.L. Luxon. A design retrospective of the DIII-D tokamak. *Nuclear Fusion*, 42(5):614, 2002.

[8] C.P.C. Wong, R. Junge, R.D. Phelps, et al. Plasma-Surface Interactions in Controlled Fusion Devices Divertor materials evaluation system at DIII-D. *Journal of Nuclear Materials*, 196:871 – 875, 1992.

[9] D.L. Rudakov, T. Abrams, R. Ding, et al. DiMES PMI research at DIII-D in support of ITER and beyond. *Fusion Engineering and Design*, page http://dx.doi.org/10.1016/j.fusengdes.2017.03.007, 2017.

[10] V. Rohde, N. Endstrasser, U.v. Toussaint, et al. Tungsten erosion by arcs in ASDEX upgrade. *Journal of Nuclear Materials*,

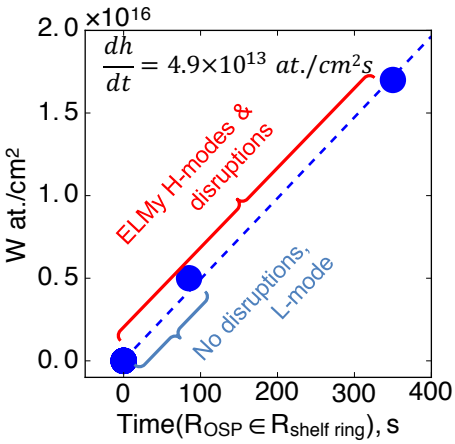

Figure 7: Scaling of W deposition during the Metal Tile Campaign in outer SOL at DiMES radius measured after a series of L-mode shots on a DiMES sample [14] and after the whole campaign on a graphite tile, i.e. both measurements made at the same poloidal coordinate.

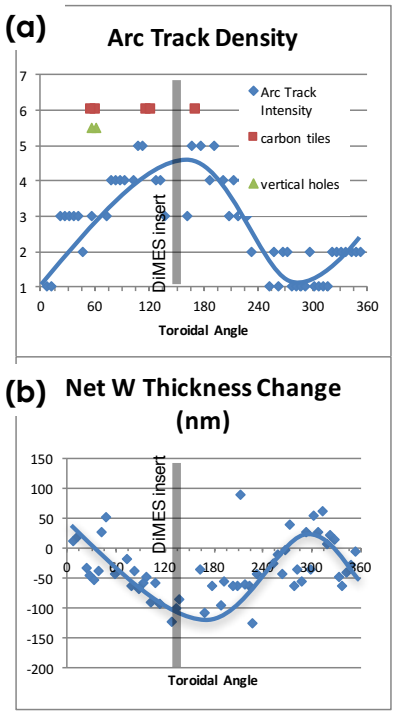

Figure 8: Toroidal variation of arc track density binned in 5 groups (a) and integrated net W erosion (b). Solid lines are to guide eye.

415(1, Supplement):S46 – S50, 2011. Proceedings of the 19th International Conference on Plasma-Surface Interactions in Controlled Fusion.

[11] E.A. Unterberg et al. Fast spectroscopic measurements of tungsten neutral flux due to plasma-material interactions using a two-filter, fiber-optic coulped diagnostic in the DIII-D divertor. 21st High-Temperature Plasma Diagnostics Conf. (Madison, USA, June 2016).

[12] E. A. Unterberg, D. M. Thomas, T. W. Petrie, et al. Overview of the DIII-D divertor tungsten rings campaign. *58th Annual Meeting of the APS division of Plasma Physics, Oct. 31-Nov. 4, 2016.*

[13] M. Mayer, M. Andrzejczuk, R. Dux, et al. Tungsten erosion and redeposition in the all-tungsten divertor of ASDEX Upgrade. *Physica Scripta*, 2009(T138):014039, 2009.

[14] W. R. Wampler, J .G. Watkins, D. L. Rudakov, et al. Measurements of tungsten migration in the DIII-D divertor. *This*

conference.

[15] B. Jüttner. Cathode spots of electric arcs. *Journal of Physics D: Applied Physics*, 34(17):R103, 2001.

[16] D. A. Humphreys and A. G. Kellman. Analytic modeling of axisymmetric disruption halo currents. *Physics of Plasmas*, 6(7):2742–2756, 1999.

[17] O. Gruber, K. Lackner, G. Pautasso, et al. Vertical displacement events and halo currents. *Plasma Physics and Controlled Fusion*, 35(SB):B191, 1993.

[18] E. M. Hollmann, N. Commaux, N. W. Eidietis, et al. Characterization of heat loads from mitigated and unmitigated vertical displacement events in DIII-D. *PoP*, 20(062501), 2013.

[19] J. Baró, J. Sempau, J.M. Fernndez-Varea, and F. Salvat. Penelope: An algorithm for monte carlo simulation of the penetration and energy loss of electrons and positrons in matter. *Nuclear Instruments and Methods in Physics Research Section B: Beam Interactions with Materials and Atoms*, 100(1):31 – 46, 1995.

[20] D. L. Rudakov, P. C. Stangeby, J. D. Elder, et al. Studies of short range tungsten migration in DIII-D divertor. In *58th Annual Meeting of the APS division of Plasma Physics, Oct. 31-Nov. 4, 2016*.